Acta Cryst. (1997). D**53**, 580–587

Comparison of the Structures of the Cubic and Tetragonal Forms of Horse-Spleen Apoferritin

THIERRY GRANIER, BERNARD GALLOIS, ALAIN DAUTANT, BÉATRICE LANGLOIS D'ESTAINTOT AND GILLES PRÉCIGOUX

Unité de Biophysique Structurale, EP534 CNRS, Université Bordeaux 1, 33405 Talence CEDEX, France. E-mail: precigou@maxime.cristal.u-bordeaux.fr

(*Received 2 December 1996; accepted 25 February 1997*)

Abstract

Horse-spleen apoferritin is known to crystallize in three different space groups, cubic $F432$, tetragonal $P42_12$ and orthorhombic $P2_12_12$. A structure comparison of the cubic and tetragonal forms is presented here. Both crystal forms were obtained by the vapor-diffusion technique and data were collected at 2.26 Å (cubic crystal) and 2.60 Å (tetragonal crystal) resolution. Two main differences were observed between these crystal structures: (i) whereas intermolecular contacts only involve salt-bridge type interactions *via* cadmium ions in the cubic structure, two types of interactions are observed in the tetragonal crystal (cadmium-ion-mediated salt bridges and hydrogen-bonding interactions) and (ii) cadmium ions bound in the threefold axes of ferritin molecules exhibit lower site-occupation factors in the tetragonal structure than in the cubic one.

1. Introduction

Ferritin was first isolated from mammalian spleen and liver by Laufberger (1937). Since then, it has been found in most living organisms, such as bacteria, fungi, plants, molluscs, insects and vertebrates. Its universal occurance as well as its fascinating ability to reversibly store and release iron ions to the living cells, have incited many studies (Theil, 1987; Crichton, 1990; Harrison *et al.*, 1991; Harrison & Arosio, 1996). Despite a sequence homology sometimes lower than 20% (Andrews *et al.*, 1992), the X-ray structures of several of these proteins showed an invariance in their secondary, tertiary and quaternary structures. Ferritin molecules are made of 24 subunits. Each of these consists of a four-helix bundle (*a*–*d*) and a fifth shorter helix (*e*) at the C terminus. The 24 bundles pack together in a 432 symmetry and form a hollow shell, which inner cavity of *ca* 80 Å diameter that can host a ferrihydrite mineral core composed of up to 4500 Fe atoms. The 432 symmetry of the molecule leads to the formation of the following.

Twelve grooved arrangements along the twofold axes are the location for haem molecules in bacterioferritins [Frolow, Kalb (Gilboa) & Yariv, 1994] and are able to host porphyrins in horse-spleen ferritin (Précigoux *et al.*, 1994), or betaines in amphibian red-cell L ferritin (Trikha, Theil & Allewell, 1995). It was suggested that glutamic residues of helix *b* which border these inner cavities participate in the nucleation of the ferrihydrite mineral core (Rice, Ford, White, Smith & Harrison, 1983).

Several experimental results have suggested that eight hydrophilic channels along the threefold axes are the entry route for iron ions into the ferritin cavity (Wade *et al.*, 1991; Treffry *et al.*, 1993; Strange, Morante, Stefanini, Chiancone & Desideri, 1993; Levy, Santambrogio, Corsi, Cozzi & Arosio, 1996).

There are also six channels along the fourfold axes whose function has not yet been identified.

Crystal structures of eukaryotic ferritins published so far, *i.e.* bullfrog red cell (Trikha *et al.*, 1995), horse spleen (Rice *et al.*, 1983; Clegg, Stanfield, Bourne & Harrison, 1980) and recombinant human-H (Lawson *et al.*, 1991), show that these proteins only crystallize in the cubic space group $F432$, except for horse-spleen ferritin which also crystallizes in the orthorhombic $P2_12_12$ and tetragonal $P42_12$ space groups. These latter crystal forms were obtained a few years ago (Harrison, 1963; Hoy, Harrison & Hoare, 1974) but X-ray data were measured only to 6 Å resolution compared to cubic crystals (2.7 Å).

We recently obtained orthorhombic and tetragonal crystals (Langlois d'Estaintot *et al.*, 1996; Granier, Gallois, Dautant, Langlois d'Estaintot & Précigoux, 1996) which diffract to higher resolution. We present here a comparison of the structures of cubic (2.26 Å resolution) and tetragonal (2.60 Å resolution) crystals of horse-spleen apoferritin.

2. Experimental

2.1. *Crystallization*

Commercial horse-spleen apoferritin (Sigma) was further purified on a gel-filtration column (a superfine Sephacryl S-300 column) in order to eliminate ferritin oligomers (Yang, Matsubara, Yamaki, Ebina & Nagayama, 1994). horse-spleen ferritin contains L- and H-type chains, with proportions of about 90 and 10%, respectively. The structures below refer to the L-type chain sequence. Eluted fractions of the monomers were pooled and concentrated up to 25 mg ml^{-1}. The protein

Table 1. *Data collection*

	Cubic	Tetragonal
Crystal size (mm)	0.6 × 0.5 × 0.6	0.5 × 0.3 × 0.25 0.5 × 0.35 × 0.25
Space group	*F*432	$P42_12$
Lattice parameters (Å)	$a = 182.9$	$a = b = 147.23$, $c = 152.58$
Synchrotron radiation beamline (LURE)	DW32	D41
Image-plate diameter (mm)	180	180
Crystal-to-film distance (mm)	200	135.6
Wavelength (Å)	0.901	1.375
No. of frames	30	147
Oscillation per frame (°)	1.0	1.2
Exposure time per frame (s)	120	240
Maximum resolution (Å)	2.25	2.5
Total no. of reflections	88762	354156
No. of unique reflections	12699	51340
Multiplicity	7.0	6.9
Reflections with $I > 2\sigma(I)$	84	62
Completeness (%)	99.3	89.5
R_{sym}	0.11 (0.41)*	0.06, 0.09
R_{merge}	—	0.118 (0.36)*

* Outer shell value.

sample was dialysed extensively against water. Crystals grew at room temperature by the hanging-drop vapor-diffusion method: drops were prepared by mixing 5 ml of protein solution with 5 ml of reservoir solution. In the case of cubic crystals, the latter was composed of 1.0 *M* ammonium sulfate, 80 m*M* cadmium sulfate and 3 m*M* sodium azide, while in the case of tetragonal crystals, its composition was 0.66 *M* ammonium sulfate, 80 m*M* cadmium sulfate and 3 m*M* sodium azide. Whereas cubic octahedral crystals appeared within one or two days, tetragonal crystals nucleated and grew after six to seven weeks or even longer. It is notable that crystallization conditions relative to both forms are very close to one another. Often cubic crystals grew in assays favoring the tetragonal form. However, the differences observed in the crystal growth kinetics, suggest that the nucleation of cubic crystals needs to be hindered so that the tetragonal phase may appear. Moreover, a pure monomer protein solution seems to be a condition necessary for obtaining the tetragonal form.

2.2. *X-ray data collection and processing*

Diffraction data were collected at room temperature, using a MAR Research image-plate detector on the synchrotron radiation source at LURE (Paris-Orsay, France). The high symmetry of the cubic form and an oscillation range of 30° resulted in a complete data set with high redundancy from one single crystal. For the tetragonal form, the higher oscillation ranges could not be completed without noticeable radiation damage, so that data sets from two different crystals were collected and merged. Data-collection characteristics are given in Table 1. Diffraction images from the cubic crystal were processed using *MOSFLM* (Leslie, Brick & Wonacott, 1986) and the *CCP*4 program suite (Collaborative Computational Project, Number 4, 1994), while those from the tetragonal crystals were processed and merged using the *XDS* package (Kabsch, 1988*a*,*b*).

2.3. *Refinement*

Both structures were refined with *X-PLOR* (Brünger, Kuriyan & Karplus, 1987) starting with the protein atom coordinates from the 2.4 Å refined cubic structure of the hematoporphyrin IX–apoferritin complex (Michaux *et al.*, 1996). Whereas the asymmetric unit of the cubic structure consists of a single protomer of 174 amino acids, that of the tetragonal structure is made of six protomers: this hexamer consists of a pair of trimers (*ABC*) and (*DEF*) related to one another by a twofold non-crystallographic symmetry (NCS) axis, the protomers of each trimer being related by a threefold NCS axis (see Fig. 1). This hexamer was generated with the appropriate cubic symmetry operations and positioned in the tetragonal unit cell, as described previously (Granier *et al.*, 1996), by molecular replacement using the program *AMoRe* (Navaza, 1994).

The cubic structure refinement was achieved according to the following procedure. A rigid-body refinement of the asymmetric unit was performed with data in the range 8–3.0 Å, followed by a simulated-annealing run using the slow-cooling protocol provided in *X-PLOR*.

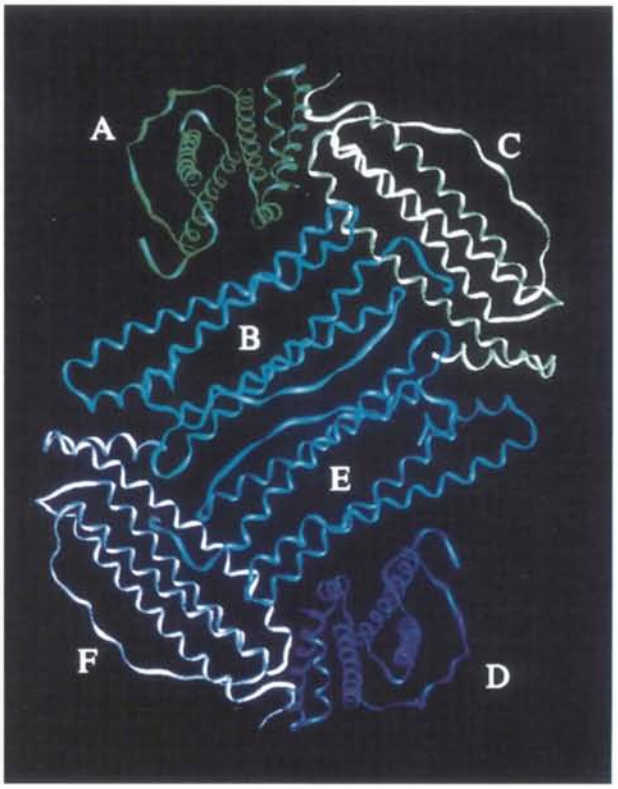

Fig. 1. The asymmetric unit of the tetragonal structure consists of six subunits, labelled here *A*–*F*.

Further refinement was carried out by increasing the resolution in steps of 0.1 Å at each cycle from 8 to 2.26 Å, alternating energy-restrained minimization and visual examination of electron-density maps (program *TURBO-FRODO*, Roussel, Fontecilla-Camps & Cambillau, 1990). All badly positioned side chains were excluded from map calculation and repositioned by real-space fitting in $(3F_o - 2F_c)$ electron-density maps. Water molecules were positioned on condition that they fit residual $(F_o - F_c)$ density peaks (having an amplitude 3σ greater than the average level of the difference map electron density) and that they satisfy hydrogen-bonding geometry with protein atoms. Individual B temperature factors were refined at the last stage, and water molecules with B factors greater than 60 Å^2 were discarded.

The tetragonal structure refinement followed the same procedure except that after rigid-body refinement of the asymmetric unit a second cycle was undertaken considering each subunit of the asymmetric unit as a rigid body. No simulated annealing was performed, and further minimization included an NCS restraint between the subunits of the hexamer, while the resolution range was increased in steps of 0.1 Å from 8 to 2.6 Å. One may notice that the lower diffracting power and resolution of the tetragonal crystals, allowed us to locate fewer solvent molecules than in the cubic structure.

The refinement of the site occupation and B factors of cadmium ions at the threefold axes of the molecule, were refined with *X-PLOR*: these two parameters which are strongly correlated, were refined in alternate runs, so that a final $(F_o - F_c)$ map, showed no residual feature at the cadmium sites.*

3. Results and discussion

3.1. *Quality of the structures*

The cubic structure was refined to a resolution of 2.26 Å with a final R factor of 0.187, while the tetragonal one was refined to a resolution of 2.60 Å with a final R factor of 0.201. The results and statistics of the refinement are summarized in Table 2: stereochemical constraints were kept tight for both structures. The overall r.m.s. random positional errors in atomic coordinates of the refined model, estimated from Luzzati plots (Luzzati, 1952), are 0.22 and 0.26 Å, for the cubic and tetragonal structures, respectively. In the tetragonal structure, because of the NCS restraint applied to the six subunits of the asymmetric unit, a superposition of the atoms of the six subunits together yields an r.m.s. deviation lower than 0.08 and 0.12 Å on main-chain and side-chain atoms, respectively.

Table 2. *Refinement statistics*

	Cubic	Tetragonal
Resolution range (Å)	8–2.26	8–2.60
R factor	0.186	0.201
Last resolution shell (Å)	2.31–2.26	2.70–2.60
R factor	0.25	0.27
σ cutoff	$[F_o > 2\sigma(F_o)]$	$[F_o > 1\sigma(F_o)]$
No. of reflections included	11870	33482
No. of protein atoms	1398	8398
No. of solvent molecules	109	272
No. of Cd^{2+} ions	3	5
R.m.s. deviations from		
Ideal bond lengths (Å)	0.017	0.012
Ideal bond angles (°)	2.9	2.4
Ideal improper angles (°)	1.9	1.7
Mean B factors (Å^2)		
Protein atoms	23.4	25.4
Main-chain atoms	20.9	23.7
Side-chain atoms	25.9	27.0
Solvent atoms	31.5	37.0

$(2F_o - F_c)$ maps contoured at the 1σ level have a continuous electron density for all backbone atoms of both structures, with the exception of residues G156 and S157, at the turn between helices D and E, and at the last two C-terminus residues H173 and D174. Fig. 2 is a plot of the real-space R factor for each residue calculated following Jones, Zou, Cowan & Kjeldgaard (1991) along with average temperature factors of side-chain and main-chain atoms. All the side chains with the weakest electron density are those of polar or ionizable residues, which are largely exposed to solvent. Among them, are those of residues E45, E53, E56, E57: these residues point toward the inner cavity of the molecule, and are believed to participate in the ferrihydrite mineral core nucleation (Harrison & Arosio, 1996, and references therein). A Ramachandran plot of both structures shows that 93.7% of non-glycine and non-proline residues are found in the most favourable regions, and the remaining 6% in additional allowed regions. The overall G factor (Morris, MacArthur, Hutchinson & Thornton, 1992; Laskowski, MacArthur, Moss & Thornton, 1993) takes the value 0.04 in the cubic structure, while for the tetragonal one, this value is 0.10, which indicates a good stereochemistry.

3.2. *General features of the subunit*

The cubic structure of horse-spleen apoferritin has been extensively described (Rice *et al.*, 1983; Harrison *et al.*, 1991 and references therein). Here we will only mention features not highlighted before, such as hydrogen bonds. Let us recall that helices in the ferritin subunit pack as antiparallel *ab* and *cd* pairs extending from T10–Y36, E45–R72, T92–A119 and P123–S157, while the fifth shorter helix E extends from residues A159 to L169. Connectivities of helices *a–b* and *c–d* are adjacent, while the connectivity of helices *b–c* which are linked by the *bc* loop, is crossed over. Loops *ab* and *cd* are type I β-turns, and the *de* loop a type III turn. Helix

* Atomic coordinates and structure factors have been deposited with the Protein Data Bank, Brookhaven National Laboratory (Reference: 1IER, R1IERSF and 1IES, R1IESSF for the cubic and tetragonal structures, respectively). Free copies may be obtained through The Managing Editor, International Union of Crystallography, 5 Abbey Square, Chester CH1 2HU, England (Reference: GR0704).

d is distorted by a π helix turn between residues L129 and L134. Inside each subunit, one observes, for both structures, 28 hydrogen bonds and eight electrostatic interactions involving side-chain atoms: these are listed in Table 3. Fig. 3 shows a ferritin subunit. Along with the trace of Cα atoms, two types of side chains are visualized: those given in Table 3, which participate in intersecondary-structure interactions, as well as those of apolar residues which belong to the hydrophobic cores buried in the four-helix bundle. The latter appears divided into alternating regions which are each of a different nature: the salt bridge built by residues Y30, K58, E137 and E103, occupies the central part of the bundle, and is bordered by two hydrophobic cores (residues V12, A15, V16, L19, L110, L113, L116, L125, F128, L129, F133 on the C-terminal side, and residues L33, V47, F50, A95, A98, A99 on the N-terminal side). Both hydrophobic cores are flanked, at each end of the bundle by regions rich in polar or charged residues which build hydrogen bonds or electrostatic interactions between different secondary-structure elements.

3.3. *Intersubunit interactions*

In the ferritin molecule, each subunit is surrounded by six subunits. However, the 432 symmetry of the molecule implies that all the interactions between subunits

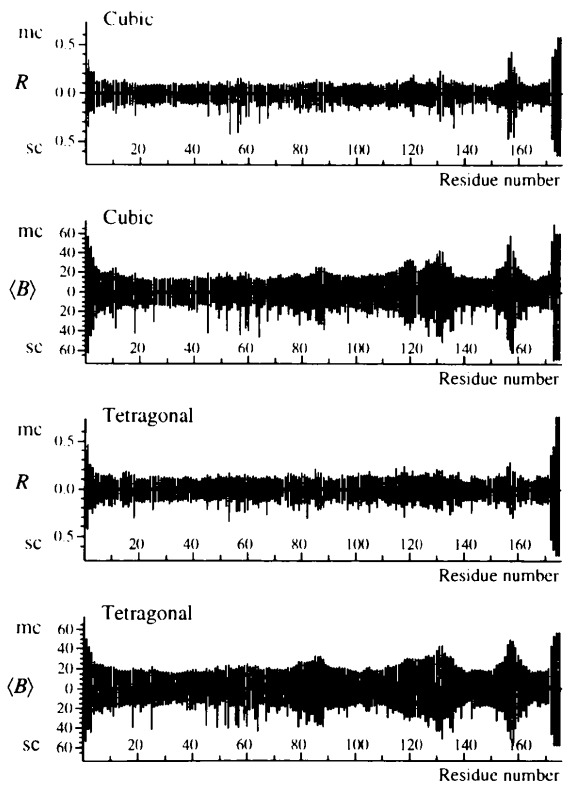

Fig. 2. Real-space *R* factor as a function of the residue number, along with the average temperature factors for the cubic structure and one chain of the tetragonal structure. (sc: side-chain atoms; mc: main-chain atoms).

Table 3. *Salt bridges and hydrogen bonds involving side-chain atoms in the ferritin subunit observed in both structures*

The program used was *hbplus* (McDonald & Thornton, 1994).

Hydrogen bonds

Side chain–main chain		Main chain–side chain		Side chain–side chain	
Donor	Acceptor	Donor	Acceptor	Donor	Acceptor
R5	Y8	I4	S2	Y8	Q69
Q69	E13	V12	S9	Y30	E103
T29	R25	R75	E13	W89	S32
R25	K83	G46	E167	T92	E163
S27	A55	T91	D94	H114	E130
C48	G34	T92	E163	K143	H147
Y36	G90	L125	D122		
R75	G74				
Q86	E88				
S105	V101				
S118	H114				
C126	D122				
S131	D127				
T149	G145				
S157	R153				

Salt bridges

R5	E13
R39	D41
R39	E88
K58	E103
R59	E60
R72	D122
K142	D146
R168	E167

Table 4. *Intersubunit hydrogen bonds and electrostatic interactions observed in both structures*

Subunits *B–E* (twofold molecular axis)

Side chain–main chain		Main chain–side chain		Side chain–side chain	
Donor	Acceptor	Donor	Acceptor	Donor	Acceptor
Y28	Q79	K83	D80	S2	D40
N70	F35			R52	E63
				N70	D38
				R75	D40
				R75	D40
				R52	E63

Main chain–main chain

L81	L81

Subunits *C–E* (fourfold molecular axis)

Side chain–main chain		Main chain–side chain		Side chain–side chain	
Donor	Acceptor	Donor	Acceptor	Donor	Acceptor
R168	L169	L161	S157	Y164	T170
K142	D38				
T149	D40				
R153	V42				

Subunits *B–C* (threefold molecular axis)

Side chain–main chain	
Donor	Acceptor
K104	Q3

are described when considering three different pairs of subunits (see Fig. 1). The interactions are listed in Table 4. It appears that the strongest interacting subunit pairs are those building a dimer (subunits *B* and *E* of Fig. 1). Less strong is a subunit pair bordering the fourfold

axis (subunits *C* and *E*). The weakest single interaction of this type is observed between subunits constituting a threefold axis. The numbers of such interactions between secondary-structure elements are listed in Table 5: the most loosely bound secondary structures are helices *c* and *d*. By contrast, helix *e* and loop *b–c* are much more closely bound to neighbors. From this point of view, the threefold axes of the molecule, bordered by helices *c* and *d*, are the looser regions of the shell. This might be due to the fact that iron ions are believed to enter the ferritin through the threefold axes. Moreover, a recent study on diffusion of small nitroxide spin probes of 7–9 Å diameter (Yang & Chasteen, 1996) showed that these rather bulky molecules are able to enter the ferritin molecule through the threefold axes, although the channels appear to be very narrow (~3 Å).

3.4. *Differences between the cubic and tetragonal structures*

Both structures are similar. A superposition of the asymmetric unit main-chain atoms of the cubic structure with each of the six chains of the tetragonal asymmetric unit shows an r.m.s. deviation smaller than 0.17 Å on main-chain atoms, and 1.1 Å on side-chain atoms. A few side chains adopted different conformations from one crystal form to the other, *i.e.* those of residues E53, R64, Q79 and Q82. Within the tetragonal structure, a few

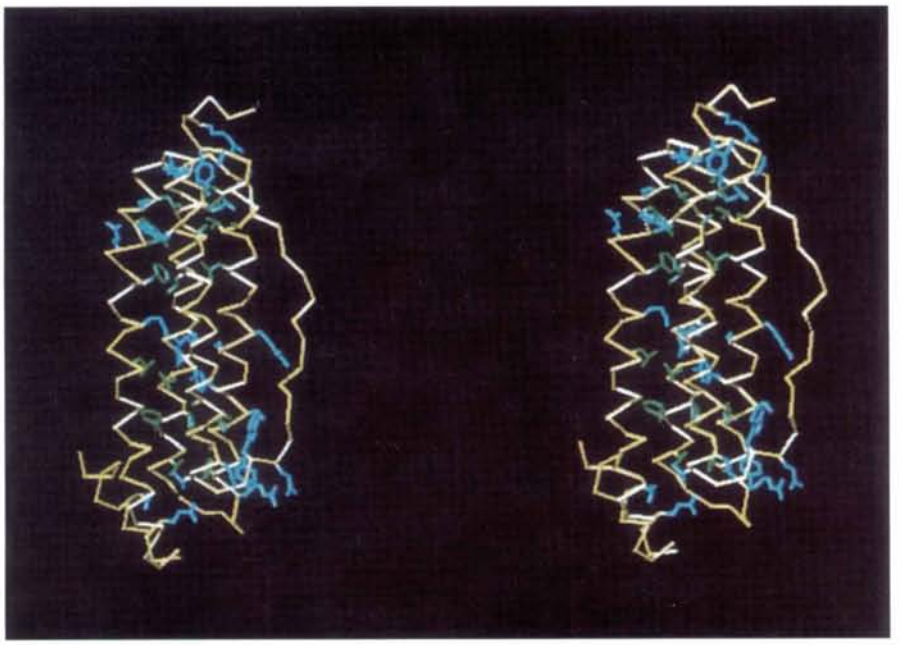

Fig. 3. Stereoview of a horse-spleen ferritin subunit (cubic structure): side chains of residues involved in hydrogen bonds or salt-bridge interactions between secondary-structure elements, are shown in blue; apolar residues which form hydrophobic clusters are shown in green.

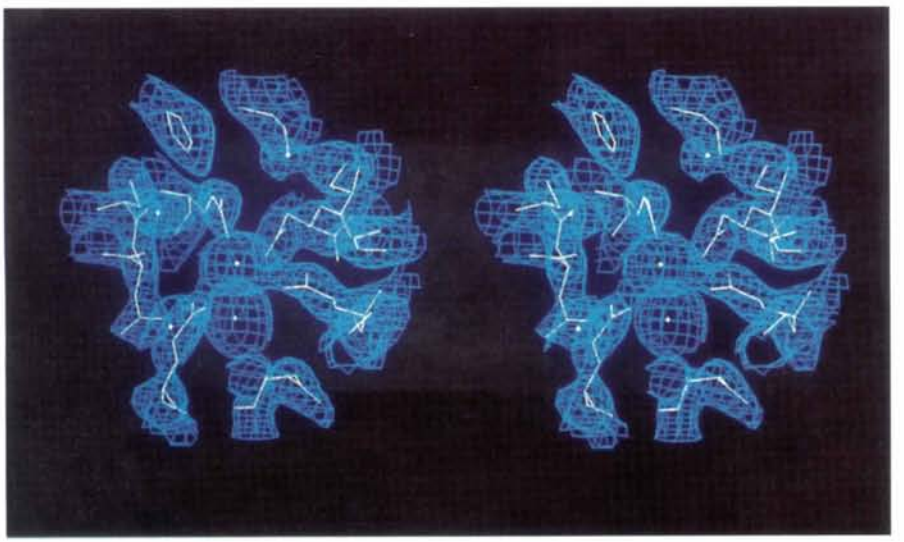

Fig. 4. Stereoview of the threefold axis: two sites are found which bind cadmium ions: site 1 which involves residues E130 (in the foreground in the picture) and site 2 which involves residues D127 (background of the picture). Electron density is shown at the 1σ level (tetragonal structure, chains *A*, *B* and *C*).

Table 5. *Number (N) of intra- and intersubunit hydrogen bonds and electrostatic interactions binding different secondary-structure elements of a ferritin subunit within the ferritin molecule*

	a	*b*	*bc*	*c*	*d*	*e*
N	11	10	9	6	6	7
N/residue	0.4	0.37	0.9	0.22	0.18	0.7

side chains, *i.e.* residues R18, H49 and K67, exhibited different conformations depending on the chain of the asymmetric unit they belong to. No NCS restraints were imposed on the latter. H49 clearly adopted an alternate conformation in the cubic structure.

However, these differences concern residues with the weakest densities (Fig. 2), and it seems difficult at such resolution (2.6 Å for the tetragonal structure) to separate signal from noise. A recent overview (Kleywegt, 1996) of structure refinement including NCS restraint suggests caution should be applied.

The major differences occuring between the two structures concern the high-density residual peaks commonly attributed to cadmium ions. At the end of the refinement, $(F_o - F_c)$ Fourier difference map revealed the presence of high-density residual peaks at the threefold axes of the ferritin molecule, near residues E130 (site 1) and D127 (site 2) (see Fig. 4): site 1 is exposed to the exterior of the protein, while site 2 is located near the inner surface of the protein shell.

These residual peaks (height greater than 10σ) were attributed to cadmium ions. Their site occupation and temperature factors have been refined so as to best fit the electron density. The values obtained are listed in Table 6, and show that the number of cadmium ions bound to the ferritin molecule at the threefold axes is significantly greater in the case of the cubic structure (12 cadmium ions) than in the tetragonal one (4.8 cadmium ions). This result should be viewed with caution, but the difference observed between both structures is large enough to be considered at least qualitatively. Cadmium ions have been reported to be inhibitors of iron uptake in ferritins. A recent study (Pead *et al.*, 1995) on metal ions binding to horse-spleen ferritin, in particular showed that Cd^{2+} binding to ferritin is strongly pH dependent: at pH 5.5, an apoferritin molecule binds three Cd^{2+} ions, whereas at pH 7.5, it binds 54 Cd^{2+} ions. In the cubic crystal, higher rate of Cd^{2+} binding could be explained by a pH difference in the crystallizing solution drop at equilibrium. The pH of the reservoir solution was 5.7 for both crystallizing conditions. The only difference concerns the ammonium sulfate concentration which is higher in the cubic crystallization set than in the tetragonal one: NH_3 molecules, which are very volatile, raise the pH to higher values by diffusion from the reservoir to the hanging drop: the higher the ammonium sulfate concentration, the higher the pH of the hanging drop at equilibrium.

Table 6. *Cadmium binding sites at the threefold axis*

	Cubic		Tetragonal	
	s.o.f.*	B (Å^2)	s.o.f.*	B (Å^2)
Site 1	0.5	20	0.25	20
			0.25	20
Site 2	1	16	0.35	20
			0.35	20

*S.o.f., site occupation factor (%).

3.5. *Crystal packing*

Whereas ferritin molecules pack in a face-centered lattice in the cubic crystal, they obey a pseudo-body-centered lattice arrangement in the tetragonal form. Therefore, intermolecular contacts involve different residues from one crystal form to the other.

In the cubic crystal, the apoferritin molecule is centered at the Wyckoff position (0,0,0) and the centers of neighboring molecules are 129.3 Å apart. In the lattice, molecules bind to one another *via* salt-bridge interactions which involve Cd^{2+} ions and residues D80 and Q82: there are 24 of these identical interactions per ferritin molecule (two per neighboring molecules), and each subunit participates in such an interaction.

In the tetragonal crystal, the apoferritin molecule is centered at the Wyckoff position (0, 0.5, 0.2583). Centers of closest neighbors are located at (0.5, 0, 0.7417) and (0.5, 0, –0.2583), *i.e.* 130.6 and 127.6 Å further apart, respectively. For each type of neighbor, a particular intermolecular contact is observed (see Figs. 5*a* and 5*b*). The first one involves chain *B* of asymmetric unit (x, y, z) and chain *C* of asymmetric unit $(1-y, 1-x, 1-z)$. A cadmium ion binds the side-chain atoms of residues E11 (OE1 and OE2) and T10 (OG1) to side-chain atoms of residues E11 (OE1 and OE2) and Q120 (NE2), while a water molecule (WAT307) is found to bind residues T10 of chains *C* and *B*. Another interaction involves residues D112 of chains *C*, *via* two water molecules (WAT211 and WAT212, see Fig. 5*a*).

In the second type of contact (Fig. 5*b*), chains *D* of asymmetric units (x, y, z) and $(1-y, 1-x, -z)$ are connected *via* a water molecule and an electrostatic interaction between residues R18 [subunit (x, y, z)], residues E11 [subunit $(1-y, 1-x, -z)$] and residues D112; the side chain of residue R18 of chain *D*, adopts a different conformation to the one observed in the other chains of the asymmetric unit. In the present case, a single ferritin molecule is bound to its neighbors by eight salt-bridge interactions involving Cd^{2+} ions and eight hydrogen-bond and electrostatic interactions. Moreover, only three chains (*B*, *C* and *D*) per asymmetric unit, *i.e.* 12 chains per molecule, are involved in close-packing interactions.

The differences between these intermolecular contacts and packings may arise from the buried surfaces between neighboring molecules in the crystal lattice. These buried surfaces are given in Table 7: it appears that the

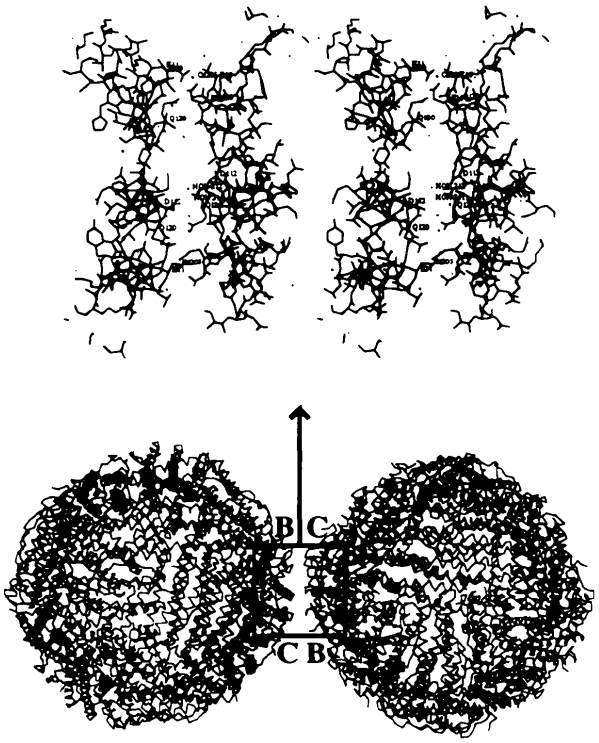

(*a*)

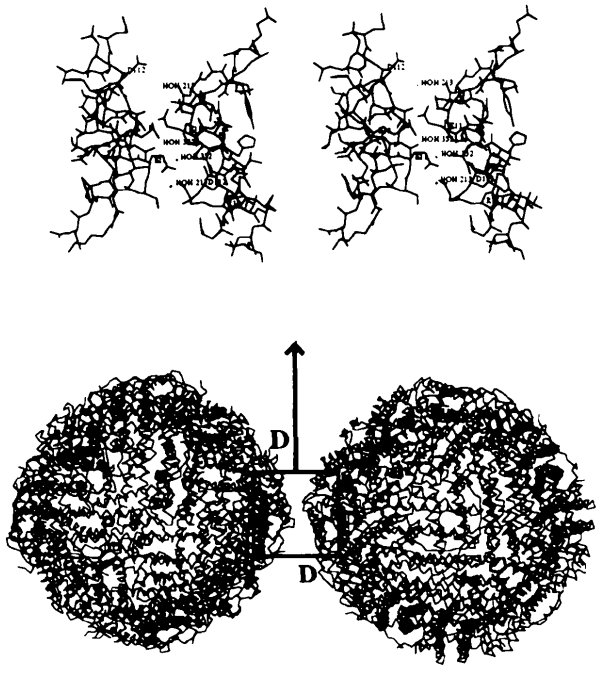

(*b*)

Fig. 5. Intermolecular contacts in the tetragonal structure: (*a*) between chain *B* of asymmetric unit (*x*, *y*, *z*) and chain *C* of asymmetric unit (1 − *y*, 1 − *x*, 1 − *z*). (*b*) Between chains *D* of asymmetric units (*x*, *y*, *z*) and (1 − *y*, 1 − *x*, − *z*).

Table 7. *Buried surface between neighboring molecules in crystal packing (Å²)*

	Side chain			Total value per
	Non-polar	Polar	Main chain	molecule
Cubic	36	97	0.1	1596
Tetragonal				
Contact*	121	157	38	1264
Contact†	152	104	6	1048

* Contacts displayed in Fig. 5(*a*). † Contacts displayed in Fig. 5(*b*).

total buried surface per molecule due to neighboring molecules is 45% greater in the tetragonal structure than in the cubic one, although the number of contacts is lower in the pseudo-body-centered lattice of the tetragonal crystal. The major increase comes from non-polar side-chain atoms, but does not correspond to the burial of particular hydrophobic residues except A119 of chains *C* and *D*. As a general trend, each type of intermolecular contacts observed involves polar or charged residues which protrude at the protein surface. The average distance of Cα atoms of residues exposed to the outer surface of the molecule, from its center, is 58.73 Å; Cα distances of residues T10, E11, D80, Q82, Q120 are 63.0, 63.3, 62.6, 60.4, 60.1 Å away from the center of the molecule, while D112 is slightly closer, *i.e.* 59.9 Å.

We are grateful to LURE (Laboratoire d'Utilisation du Rayonnement Electromagntique, Orsay, France) for providing us with facilities on beamlines DW32 and D41 and, in particular, to R. Fourme and A. Levitt-Bentley for their assistance during data collection.

References

Andrews, S. C., Arosio, P., Bottke, W., Briat, J. F., von Darl, M., Harrison, P. M., Laulhere, J. P., Levi, S., Lobreaux, S. & Yewdall, J. (1992). *J. Inorg. Biochem.* **47**, 161–174.

Brünger, A. T., Kuriyan, J. & Karplus, M. (1987). *Science*, **235**, 458–460.

Clegg, G. A., Stanfield, R. F. D., Bourne, P. E. & Harrison, P. M. (1980). *Nature (London)*, **288**, 298–300.

Collaborative Computational Project, Number 4 (1994). *Acta Cryst.* D**50**, 760–763.

Crichton, R. R. (1990). *Adv. Protein Chem.* **40**, 281–361.

Frolow, F., Kalb (Gilboa), A. J. & Yariv, J. (1994). *Nature Struct. Biol.* **1**, 453–460.

Granier, T., Gallois, B., Dautant, A., Langlois d'Estaintot, B. & Précigoux, G. (1996). *Acta Cryst.* D**52**, 594–596.

Harrison, P. M. (1963). *J. Mol. Biol.* **6**, 404–422.

Harrison, P. M., Andrews, S. C., Artymiuk, P. J., Ford, G. C., Guest, J. R., Hirzmann, J., Lawson, D. M., Livingstone, J. C., Smith, J. M. A., Treffry, A. & Yewdall, S. J. (1991). *Adv. Inorg. Chem.* **36**, 449–486.

Harrison, P. M. & Arosio, P. (1996). *Biochem. Biophys. Acta*, **1275**, 161–203.

Hoy, T. G., Harrison, P. M. & Hoare, R. J. (1974). *J. Mol. Biol.* **86**, 301–308.

Jones, T. S., Zou, J. Y., Cowan, S. W. & Kjeldgaard, M. (1991). *Acta Cryst.* A**47**, 110–119.
Kabsch, W. (1988*a*). *J. Appl. Cryst.* **21**, 67–71.
Kabsch, W. (1988*b*). *J. Appl. Cryst.* **21**, 916–924.
Kleywegt, G. J. (1996). *Acta Cryst.* D**52**, 842–857.
Langlois d'Estaintot, B., Dautant, A., Granier, T., Gallois, B., Michaux, M. A. & Précigoux, G. (1996). *Acta Cryst.* D**52**, 597–600.
Laskowski, R. A., MacArthur, M. W., Moss, D. S. & Thornton, J. M. (1993). *J. Appl. Cryst.* **26**, 283–291.
Laufberger, E. V. (1937). *Bull. Soc. Chim. Biol.* **19**, 1576–1582.
Lawson, D. M., Artymiuk, P. J., Yewdall, S. J., Smith, J. M. A., Livingstone, J. C., Treffry, A., Luzzago, A., Levi, S., Arosio, P., Cesarini, G., Thomas, C. D., Shaw, W. V. & Harrison, P. M. (1991). *Nature (London)*, **349**, 541–544.
Leslie, A. G., Brick, P. & Wonacott, A. J. (1986). *CCP4 News*, **18**, 33–39.
Levy, S., Santambrogio, P., Corsi, B., Cozzi, A. & Arosio, P. (1996). *Biochem. J.* **317**, 467–473.
Luzzati, V. (1952). *Acta Cryst.* **5**, 802–810.
Morris, A. L., MacArthur, M. W., Hutchinson, E. G. & Thornton, J. M. (1992). *Proteins*, **12**, 345–364.
Michaux, M. A., Dautant, A., Gallois, B., Granier, T., Langlois d'Est aintot, B. & Précigoux, G. (1996). *Proteins Struct. Funct. Genet.* **34**, 314–321.
Navaza, J. (1994). *Acta Cryst.* A**50**, 157–163.
Pead, S., Durrant, E., Webb, B., Larsen, C., Heaton, D., Johnson, J. & Watt, G. D. (1995). *J. Inorg. Biochem.* **59**, 15–27.
Précigoux, G., Yariv, J., Gallois, B., Dautant, A., Courseille, C. & Langlois d'Estaintot, B. (1994). *Acta Cryst.* D**50**, 739–743.
Rice, D. W., Ford, G. L., White, J. L., Smith, J. M. A. & Harrison, P. M. (1983). *Adv. Inorg. Biochem.* **5**, 39–49.
Roussel, A., Fontecilla-Camps, J. C. & Cambillau, C. (1990). *Acta Cryst.* A**46**(suppl), C66.
Strange, R., Morante, S., Stefanini, S., Chiancone, E. & Desideri, A. (1993). *Biochem. Biophys. Acta*, **1164**, 331–334.
Theil, E. C. (1987). *Annu. Rev. Biochem.* **56**, 289–315.
Treffy, A., Bauminger, E. R., Hechel, D., Hodson, N. W., Nowik, I. & Yewdal, S. J. (1993). *Biochem. J.* **293**, 721–728.
Trikha, J., Theil, E. C. & Allewell, N. M. (1995). *J. Mol. Biol.* **248**, 949–967.
Wade, V. J., Levi, S., Arosio, P., Treffry, A., Harrison, P. M. & Mann, S. (1991). *J. Mol. Biol.* **221**, 1443–1452.
Yang, D., Matsubara, K., Yamaki, M., Ebina, S. & Nagayama, K. (1994). *Biochem. Biophys. Acta*, **1206**, 173–179.
Yang, X. & Chasteen, N. D. (1996). *Biophys. J.* **71**, 1587–1595.